Available online at www.sciencedirect.com
ScienceDirect
International Journal of Solids and Structures 44 (2007) 2442–2457
INTERNATIONAL JOURNAL OF SOLIDS and STRUCTURES
www.elsevier.com/locate/ijsolstr

The dynamic response of composite sandwich beams to transverse impact

V.L. Tagarielli, V.S. Deshpande, N.A. Fleck *

Cambridge University, Engineering Department, Trumpington Street, Cambridge CB2 1PZ, UK

Received 9 August 2005; received in revised form 12 July 2006
Available online 22 July 2006

Abstract

The dynamic response of glass fibre–vinylester composite beams is measured by impacting the beams at mid-span with metal foam projectiles. The beams exist in composite monolithic form, and in sandwich configuration with composite face-sheets and a core made from PVC foam or end-grain balsa wood. High-speed photography is used to measure the transient transverse deflection of the beams and to record the dynamic modes of deformation and failure. For both monolithic and sandwich configurations, a flexural wave travels from the impact site towards the supports. Ultimate failure of the monolithic and sandwich beams is by tensile tearing of the faces. The sandwich beams also exhibit cracking of the core, and face-sheet delamination. The dynamic strength of the beams is quantified by the maximum transient transverse deflection at mid-span of the beams as a function of projectile momentum. It is demonstrated that sandwich beams can outperform monolithic beams of equal mass. The trade-off between core strength and core thickness is such that a low density PVC foam core outperforms a higher density PVC foam core. End-grain balsa wood has a superior stiffness and strength to that of PVC foam in compression and in shear. Consequently, sandwich beams with a balsa core outperform beams with a PVC foam core for projectiles of low momentum. The order reverses at high values of projectile momentum: the sandwich beams with a balsa wood core fail prematurely in longitudinal shear by splitting along the grain.

Keywords: Composite sandwich panels; Dynamic testing; PVC foam; Balsa wood

1. Introduction

Sandwich beams with composite face-sheets and a lightweight foam core are commonly used in lightweight structures. Thus, it is important to ascertain their deformation and fracture behaviour under both static and dynamic loadings. A significant body of literature now exists on the measured and predicted properties of composite sandwich structures under static loading. For example, Steeves and Fleck (2004) have investigated the static three-point bending response of simply supported sandwich beams made from glass–epoxy face-sheets and a polymer foam core. Tagarielli et al. (2004) have investigated the effect of fully clamped boundary

* Corresponding author. Tel.: +44 1223 332650; fax: +44 1223 765046.
E-mail address: naf1@eng.cam.ac.uk (N.A. Fleck).

0020-7683/$ - see front matter
doi:10.1016/j.ijsolstr.2006.07.015

conditions upon the static bending response of these beams. The main modes of deformation and failure under static loading are reviewed in the books of Zenkert (1995), Gibson and Ashby (1997) and Ashby et al. (2000) while Abrate (1998) has summarised the failure of composite structures under impact loading.

The behaviour of composite sandwich structures subjected to low speed impact is fairly well understood. In the aerospace industry, the focus of attention has been mainly upon barely visible impact damage due to slow speed impact. For example, delamination and a consequent reduction of compressive strength can be observed upon dropping a wrench on a composite structure, see for example Olsson et al. (in press). Likewise, in the automotive industry, the concern is with relatively low impact speeds (on the order of 10–30 m s^{-1}). Recently, Xu and Rosakis (2000) have performed an experimental investigation into the delamination failure of composite sandwich beams in this velocity range.

In a broad range of practical engineering applications, structures are subjected to intense, distributed loading over a short time, such that the applied loads far exceed the quasi-static collapse strength. The response of metallic monolithic beams and plates to shock type loading has been extensively investigated. For example, Wang and Hopkins (1954) and Symmonds (1954) analysed the impulsive response of clamped circular plates and beams, respectively. An increasing body of theoretical work suggests that metallic sandwich structures are more resistant to shock loading than monolithic structures, see for example Fleck and Deshpande (2004) and Xue and Hutchinson (2003). The superior performance of the metallic sandwich structure is due in part to fluid–structure interaction effects, as outlined by Taylor (1941).

The prediction of enhanced dynamic strengths of *metallic* sandwich beams over monolithic designs has been confirmed in a number of recent experimental investigations. In these studies, sandwich structures were subjected to high intensity pressure pulses by impact with metal foam projectiles (Radford et al., 2005). The pressure pulses applied by the projectile on the structure mimic shock loading in air and in water, with peak pressures of the order of 100 MPa and loading times of approximately 0.1 ms. Using this technique, Radford et al. (in press) and Rathbun et al. (in press) have confirmed the enhanced dynamic strengths of metallic sandwich beams with lattice cores, while McShane et al. (in press) came to the same conclusion for metallic circular sandwich plates.

Much less is known about the resistance of composite sandwich structures to *intense, distributed* dynamic loading representative of air and water blast. Olsson et al. (2006) and Moyer et al. (1991) performed finite element (FE) calculations to investigate the shock response of GRP (glass reinforced polymer) sandwich structures with the effects of fluid–structure interaction neglected. Mäkinen (2001) extended these numerical studies to underwater shock loading and demonstrated that the acoustic mismatch between the water and composite face-sheets enhances the fluid–structure interaction effect, thereby increasing the resistance of composite sandwich beams to underwater shock loading. Experimental investigations on military applications of composite structures have focused mainly on their perforation resistance to sharp projectiles; see for example the monograph of Abrate (1997). Data on the shock loading of composite sandwich structures remains lacking.

The aim of the current experimental study is to investigate the dynamic strength of composite sandwich beams comprising glass–vinylester composite face-sheets and cores made from PVC foam or end-grain balsa wood. These material combinations are commonly used in minesweeping ships and are hence of considerable practical interest. In the current study, metal foam projectiles are used to dynamically load end-clamped monolithic and sandwich beams as sketched in Fig. 1. The monolithic beams comprise plain woven glass fibre–vinylester composite, while the composite sandwich beams have face-sheets made from glass fibre–vinylester and cores made from PVC foam or balsa wood. The primary objectives of the experimental investigations are

(i) to investigate the dynamic deformation and failure mechanisms, and
(ii) to develop an understanding for the effect of core composition and sandwich beam geometry upon the dynamic strength of composite sandwich beams.

Several of the sandwich and monolithic beams are chosen to have approximately equal areal mass, allowing us to compare the dynamic strength of the beams on the basis of equal mass. First, the relevant mechanical properties of the constituent materials are reported, and the fabrication of the sandwich beams is detailed.

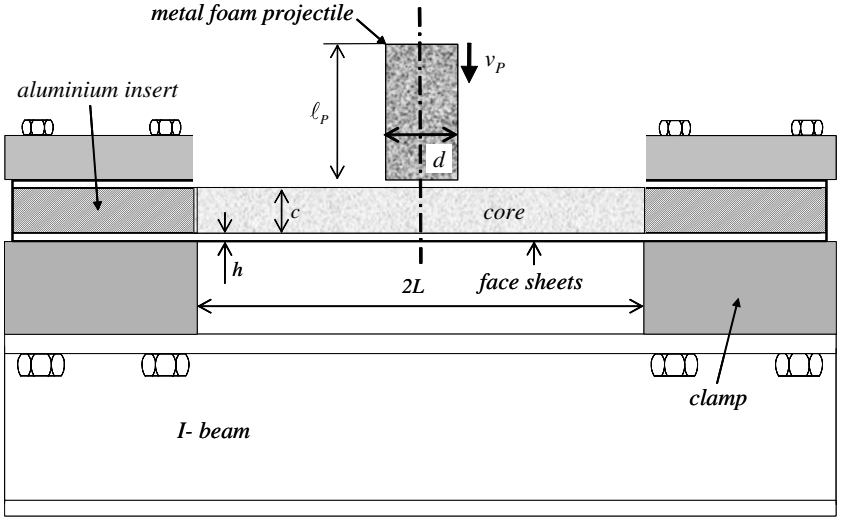

Fig. 1. Sketch of the sandwich beam geometry, with loading and clamping configuration.

Next, the dynamic beam tests are reported. Finally, we use the experimental results to deduce the role of sandwich beam geometry and core material in dictating the dynamic strength of composite sandwich beams.

2. Fabrication of the sandwich beams

The monolithic and sandwich beams tested in this study were produced by a vacuum infusion technique: a dry pre-form of woven glass fibre and core (when present) was placed under vacuum and infused by a cold-curing vinylester resin.[1] The face-sheets comprised 1–3 layers of a quasi-isotropic woven glass fibre fabric DBLT850 (of thickness 0.85 mm per layer, with equal amounts of fibres in the 0°, ±45° and 90° directions). Upon infusion with the vinylester resin an overall density of 1700 kg m^{-3} was achieved. Sandwich beams were manufactured using three types of sandwich cores as supplied by DIAB[2]; (i) grade H100 Divinycell PVC foam core (density 100 kg m^{-3}), (ii) grade H250 Divinycell PVC foam core (density 250 kg m^{-3}) and (iii) end-grain balsa wood (DIAB designation ProBalsa LD7, density 90 kg m^{-3}). Typically, panels of dimension 2 m × 1.5 m were manufactured and sandwich beams were subsequently cut from these panels using a diamond grit saw.

Monolithic beams of thickness 1.5 mm and 2.2 mm were manufactured from two and three layers of woven glass fibre fabric, respectively. Combinations of face-sheets and core for the sandwich beams were chosen as follows. The face-sheet thickness was $h = 0.85$ mm, 1.5 mm and 2.20 mm, corresponding to single, double and three layers, respectively, of the woven glass fibre fabric. The three types of sandwich core were each of thickness $c = 5$ mm, 10 mm and 15 mm. This allowed for various combinations of core and face-sheet thickness to produce three sets of sandwich beam, such that each set has an almost constant areal mass m.

The geometry and areal mass of the monolithic and sandwich beams are detailed in Table 1. We denote the monolithic beams by the letter M while the H100, H250 and balsa wood core sandwich beams are labelled H, HD and B, respectively. Note that each set is not populated by all types of beams, due to limitations on the range of availability of core densities and core thicknesses. For example, no H250 core sandwich beams are present in Set 1, and Set 3 contains neither sandwich beams with a balsa wood core nor monolithic beams. The 1.5 mm thick monolithic beams ($m \approx 2.5$ kg m^{-2}) have no corresponding sandwich beams of approximately equal areal mass and are assigned Set 0 in Table 1.

[1] The authors are grateful to Prof. D. Zankert of the Institute of lightweight Structures, KTH, Stockholm, Sweden for the use of his facilities for specimen preparation.

[2] DIAB AB, Box 201, 312 22 Laholm, Sweden.

Table 1
The materials and geometry of the sandwich beams tested in this study (the span between outer supports is $2L = 200$ mm in all tests)

	Core	Beam designation	Face-sheet thickness, h (mm)	Core thickness, c (mm)	Areal density, m (kg m^{-2})
Set 0, $m \approx 2.5$ kg m^{-2}	None	M1	0.85	–	2.55
Set 1, $m \approx 3.5$ kg m^{-2}	None	M2	1.5	–	3.74
	H100 PVC	H1	0.85	5	3.39
	Balsa	B1	0.85	5	3.43
Set 2, $m \approx 4.3$ kg m^{-2}	H100 PVC	H2	0.85	15	4.39
	H250 PVC	HD1	0.85	5	4.14
	Balsa	B2	0.85	15	4.33
Set 3, $m \approx 6.3$ kg m^{-2}	H100 PVC	H3	1.5	10	6.10
	H250 PVC	HD2	0.85	15	6.64
	H250 PVC	HD3	1.5	5	6.35

The specimens labelled M denote monolithic beams, H and HD denote sandwich beams with H100 and H250 PVC foam cores, respectively, and the specimens labelled B denote sandwich beams with a balsa wood core. The specimens are grouped in four sets, with beams of each set having approximately equal areal mass.

3. Quasi-static properties of the constituent materials

The quasi-static properties of the constituent materials were measured by performing uniaxial tension and compression tests on the composite face-sheet material, and uniaxial compression tests on the core materials.

3.1. Uniaxial tests on face-sheet materials

The tests on the composite face-sheets were conducted in a screw-driven test machine at a nominal applied strain rate of 10^{-3} s^{-1}. Rectangular specimens 120 mm × 25 mm were cut from the single layer and double layer composite sheets, and aluminium tabs were adhered to the specimen ends in order to produce test specimens with a gauge length 100 mm. The tension tests were performed by friction gripping of the aluminium end tabs. A Celanese rig was used to ensure adequate alignment in the compression tests. The axial strain in both the compression and tension tests was measured by bonding foil strain gauges to the specimens. The axial load was measured by the load cell of the test machine.

The tensile and compressive nominal stress versus nominal strain responses of the woven glass–vinylester composite are plotted in Fig. 2a (for both single and double fabric layers). In tension, the materials exhibit an initial elastic response with a modulus E_f of 9 GPa and 14 GPa for the single and double fabric layer materials, respectively. At a strain of approximately 0.5%, matrix cracking initiates and this results in a reduction of stiffness; a linear response ensues and the composite fails by tensile tearing at a tensile strain of approximately 2.5%. The tensile strength is $\sigma_f = 330$ MPa for the double layer, and 220 MPa for the single layer. In compression, the laminate displays an approximately linear response, with a compressive axial modulus slightly less than the tensile value, and this is ascribed to a combination of fibre waviness and minor misalignment of the specimen in the rig. The micro-buckling compressive strengths are approximately 150 MPa and 200 MPa for the single layer and double layer materials, respectively, and are attained at a nominal compressive strain of 1.6%. The composite specimens made from three fabric layers have similar properties to those of the double layer and so these results are omitted in Fig. 2a for the sake of clarity. It is argued that the small difference in properties between the single and multiple fabric layer materials is due to differences in the fibre volume fractions in these materials.

3.2. Compression tests on PVC foams and end-grain balsa wood

Compression tests were performed on the H100 and H250 PVC foams and on the balsa wood at a nominal strain rate of 10^{-4} s^{-1} using a screw-driven test machine. The compressive load was measured by the load cell

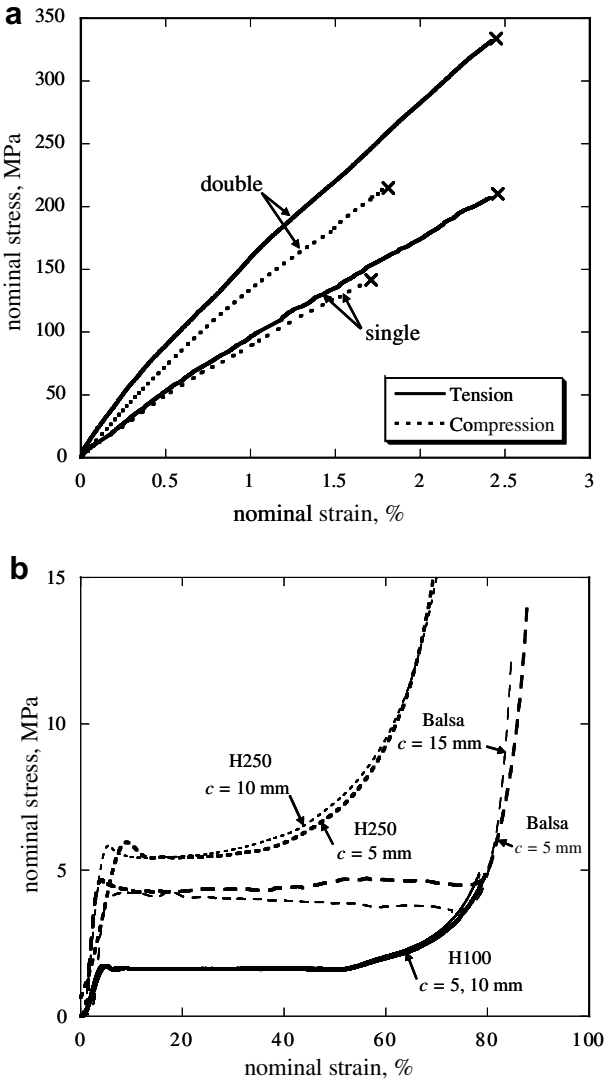

Fig. 2. The quasi-static responses of the sandwich beam constituent materials. (a) Uniaxial tensile and compressive responses of the single and double layer woven glass–vinylester laminates. (b) Uniaxial compressive response of H100 and H250 PVC foams and balsa wood.

of the test machine, while the compressive strain was deduced from the relative displacement of the compression platens, as measured by a laser extensometer. The platens were lubricated with silicone spray to reduce friction. Cuboidal specimens of cross-section 30 mm × 30 mm and thickness in the range 5–16 mm were employed. For the case of the end-grain balsa wood, care was taken to ensure that the specimens did not span the glued interfaces of the plates, so that the measured properties represent true balsa wood properties. All balsa specimens were cut from blocks with a density of about 90 kg m^{-3} in order to ensure a consistent set of results.

Fig. 2b presents a summary of the static uniaxial compressive responses for the three materials, measured at a strain rate of 10^{-4} s^{-1}. The figure includes the measured engineering stress versus strain curves for the Divinycell H100 foam, H250 foam and ProBalsa LD7 balsa wood (specimens of thickness 5 mm and 15 mm). In all cases, the material exhibits an initial elastic regime, followed by a plateau phase and densification. The static compressive strength σ_{pl} of the materials is defined here as the stress at a total strain of 15%. This strength is independent of specimen thickness and is found to be 1.7 MPa, 5.8 MPa and 4.5 MPa for the

H100, H250 and balsa wood, respectively, in line with the properties reported in the manufacturer's data sheets. The nominal densification strain is 80% for the H100 foam and the balsa wood, and about 70% for the H250 foam. While balsa wood displays a flat plateau regime up to densification, the PVC foams exhibit some hardening prior to densification. Almost no lateral expansion was observed in the plastic range in any of the compression tests. We note that these results are consistent with the previous findings of Deshpande and Fleck (2001) for the PVC foams and Tagarielli et al. (2005) for the balsa wood; readers are referred to these studies for details on the multi-axial properties of these core materials.

3.3. Strain rate sensitivity of the core materials

The uniaxial data relate to low rates of strain, while dynamic tests on beams involve much higher rates of strain. Thus, it is important to determine the strain rate sensitivity of the constituent solids. Glass fibre laminates have a negligible strain rate sensitivity: when the strain rate is increased from $10^{-4}\ s^{-1}$ to $10^{3}\ s^{-1}$, the modulus and strength increase by less than 10% (Harding and Welsh, 1983).

The strain rate sensitivity of the H100 and H250 Divinycell PVC foams and the ProBalsa LD7 has been investigated by Tagarielli et al. (in press) in a parallel study. They performed a series of uniaxial compression experiments at strain rates from $10^{-4}\ s^{-1}$ to $4000\ s^{-1}$. The high strain rate experiments were performed in a Split-Hopkinson bar apparatus comprising magnesium bars: the low modulus of magnesium confers adequate sensitivity of strain measurement in the bars for measurements on foams and woods. Their data for the compressive strain rate sensitivity of these three materials is summarised in Fig. 3. In this figure the plateau stress σ_{pl} (defined as the material strength at a total compressive strain of 15%) is plotted as a function of the applied compressive strain rate $\dot{\varepsilon}$. The experimental data for compressive strength as a function of strain rate are adequately approximated by power-law fits of the form

$$\frac{\sigma_{\mathrm{pl}}}{\sigma_0} = \left(\frac{\dot{\varepsilon}}{\dot{\varepsilon}_0}\right)^m, \tag{1}$$

where $\dot{\varepsilon}_0$ is a reference strain rate, σ_0 a reference stress, and m is the power law exponent. With the reference strain rate chosen as $\dot{\varepsilon}_0 = 1\ s^{-1}$, a least-squares fit to the experimental data provides the coefficients and m. These values are listed in Table 2 and the corresponding fits are included in Fig. 3 (for $\dot{\varepsilon} > 10^{-2}\ s^{-1}$). The compressive yield strength of the H250 PVC foam and balsa wood doubles when the strain rate is increased from quasi-static rates ($10^{-4}\ s^{-1}$) to rates on the order of $10^{3}\ s^{-1}$. In contrast, the H100 PVC foam displays only a small elevation in uniaxial compressive strength (about 30%) for the same increase in strain rate.

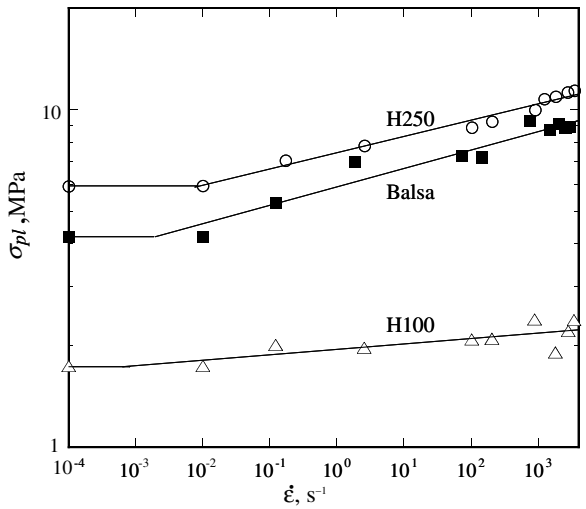

Fig. 3. Summary of the strain rate sensitivity of the PVC foams and balsa wood under uniaxial compression (Tagarielli et al., in press). The plateau stress σ_{pl} (defined as the flow stress at a total strain of 15%) is plotted against the applied strain rate.

Table 2
The power-law coefficients (1) employed to fit the experimental data for the high strain rate compression of the PVC foams and balsa wood in Fig. 3

Core material	σ_0	m
H100	1.95	0.016
H250	7.44	0.048
Balsa	5.87	0.056

In all cases a reference strain rate $\dot{\varepsilon}_0 = 1\ s^{-1}$ is chosen. Reproduced from Tagarielli et al. (in press).

4. The protocol for dynamic tests on beams

Recall that the clamped beam set-up is sketched in Fig. 1. All beams tested in this study had a total span $2L = 200$ mm and width $b = 30$ mm. The ends of the beams were rigidly clamped over a length of 75 mm, in order to constrain them against both end rotation and end displacement. The cores of the sandwich beam were replaced by aluminium inserts over the 75 mm clamped portion to allow for a high level of clamping pressure.

Aluminium alloy foam projectiles were used to provide impact loading of the clamped monolithic and sandwich beams over a central circular patch of diameter d, as shown in Fig. 1. The use of foam projectiles as a means of providing well-characterised pressure versus time has recently been developed by Radford et al. (2005) and subsequently employed to investigate the dynamic response of metallic sandwich beams and plates with lattice cores. The underlying principle of this experimental technique is that a foam projectile exerts a rectangular pressure versus time history on a rigid target. The pressure and the duration of the pressure pulse are given by (Radford et al., 2005)

$$p_0 = \sigma_c + \frac{\rho_p v_p^2}{\varepsilon_D} \tag{2}$$

and

$$\tau = \frac{l_p \varepsilon_D}{v_p}, \tag{3}$$

respectively, where ρ_p and l_p are the projectile density and length respectively while σ_c and ε_D are the foam plateau strength and nominal densification strain, respectively. Thus, the pressure and the duration of the pulse can be adjusted independently by varying the projectile velocity v_p and length l_p. Here, we conduct a series of experiments on each beam configuration by varying v_p, with all other foam projectile parameters held fixed.

Circular cylindrical projectiles of length $l_p \approx 40$ mm and diameter $d = 28.5$ mm were electro-discharge machined from Alporas aluminium foam blocks of density $\rho_p \approx 300\ kg\ m^{-3}$ (giving a projectile mass $m_p \approx 7.5 \times 10^{-3}$ kg). Recall that the beams have a width $b = 30$ mm. Thus, the projectiles load the beams over nearly their entire width. The projectiles were fired from a 28.5 mm diameter bore, 4.5 m long gas gun at a velocity v_p in the range 50–350 $m\ s^{-1}$, providing a projectile momentum per unit area $I_0 = \rho_p l_p v_p$ of up to approximately 3700 $N\ s\ m^{-2}$. Four to six tests at selected values of I_0 were conducted on each of the beam configurations listed in Table 1. In the tests, the value of I_0 was gradually increased until complete tensile failure of the beams was observed.

High-speed photography was used to observe the dynamic transverse deformation of the beams and extract the mid-span deflection versus time histories. A Hadland Imacon-790 image-converter camera was used; this is capable of taking up to 20 frames at a maximum rate of 10^7 frames s^{-1}. Inter-frame times of 100 μs and exposure times of 20 μs were used.

5. Results from dynamic tests on beams

At least four levels of impulse I_0 were applied to each beam configuration by varying the foam projectile velocity v_p. The deformation modes and deflection time histories of the back face were recorded using high

speed photography, and a post-test visual examination was also conducted. Pronounced elastic spring-back occurred after each test. Consequently, the high speed photography was essential for measuring the transient deformation and for detecting the sequence of failure events. Post-test examination was useful in confirming the existence of the various failure modes.

The main results from the experimental study are summarised in Figs. 4 and 5 for the monolithic and sandwich beams, respectively. In these figures, the maximum back-face displacement $w_{\max}$ at mid-span of each beam is plotted as a function of the initial momentum I_0 of the foam projectile. The critical momentum beyond which face-sheet tensile tearing resulted in complete failure of the beam are included in Figs. 4 and 5.

The degree of core compression is small in all sandwich beam tests, and hence the front and rear face deflections of the beams are comparable. This contrasts with the quasi-static three-point bending response of nominally identical sandwich beams, as investigated by Tagarielli et al. (2004). They observed core indentation in all tests. The difference in behaviour is attributed to the strain rate sensitivity of the PVC foams and balsa, as shown in Fig. 3.

The maximum back face deflection $w_{\max}$ of the two monolithic beams (thicknesses 0.85 mm and 1.5 mm) are approximately equal within experimental scatter (Fig. 4). In contrast, Fig. 5 shows that the sandwich beam response is sensitive to both geometry and core composition. The core thickness has a dominant effect upon impact resistance. Three examples illustrate this.

(i) The H2 beams outperform the H3 beams despite the fact that the H3 beams have higher aerial mass and thicker face-sheets (Fig. 5a).
(ii) The HD2 beams have a higher dynamic strength than the HD3 beams (Fig. 5b). Both beams have approximately the same areal mass but the HD2 beams have thicker cores.
(iii) The B2 balsa wood core beams ($c = 15$ mm) outperform the B1 ($c = 5$ mm) balsa wood core beams (see Fig. 5c). However, the effect cannot be attributed solely to the core thickness as the B2 beams have a higher areal mass than the B1 beams.

In Section 5.1, details on the dynamic modes of deformation and failure are given for each type of beam in turn. A comparison of behaviours for beams of equal mass follows in Section 5.2. This comparison instructs our search for the appropriate core and geometry to maximise impact resistance of a beam of given mass.

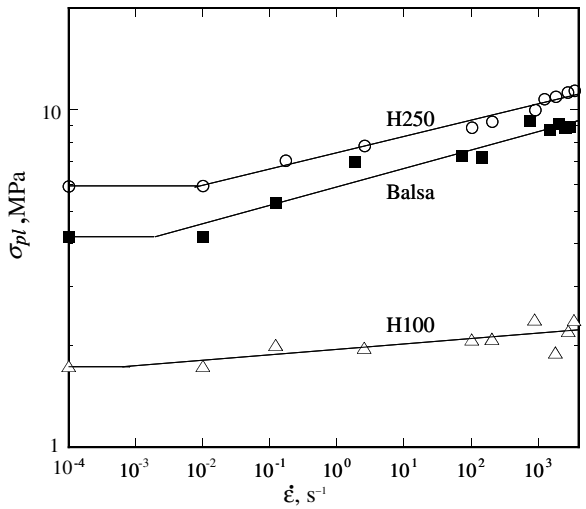

Fig. 4. The measured maximum deflection at the mid-span of the single and double layer woven glass–vinylester monolithic composite beams, as a function of the foam projectile momentum I_0. Fits to the experimental data using a power law relation are included.

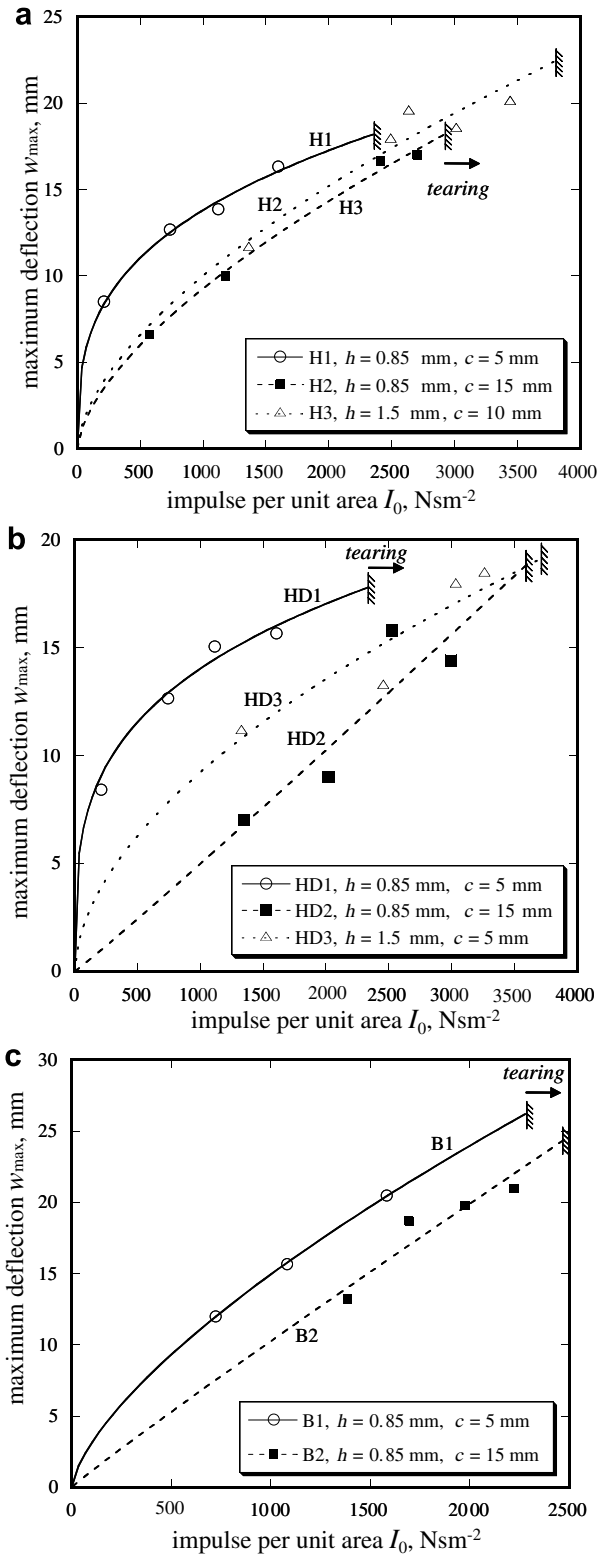

Fig. 5. The measured maximum deflection at the mid-span of the (a) H100 PVC foam core, (b) H250 PVC foam core and (c) balsa wood core sandwich beams, as a function of the foam projectile momentum I_0. Fits to the experimental data using a power law relation are included.

5.1. Deformation and failure modes for each type of beam

5.1.1. Monolithic beams

A sequence of high-speed photographs at 100 μs intervals is shown in Fig. 6a, for the monolithic specimen M1 of Table 1 impacted at $v_p = 84\ \mathrm{m\ s^{-1}}$. Impact occurs between frames 1 and 2, and by frame 3 the metal foam projectile has shortened by nearly 50% due to the propagation of a plastic shock wave along the axis of the foam from the impacted face. After frame 3, the plastic wave within the foam projectile has arrested and thereafter the projectile and the underlying beam elements share a common velocity. Between frames 2 and 4, a flexural wave travels along the beam from the impact site towards the supports. This wave is then reflected, compare frames 9 and 10. The mid-span deflection versus time history, as inferred from the high-speed photographs of Fig. 6a, is plotted in Fig. 6b. The numerical labels on the curve denote the frames of Fig. 6a. Maximum deflection is attained after approximately 500 μs. Subsequently, reflection of the flexural wave leads to elastic recovery.

5.1.2. PVC foam core sandwich beams

High-speed photographic sequences (100 μs inter-frame time) of the H100 PVC foam core sandwich beams (specimen type H2) impacted at $v_p = 204\ \mathrm{m\ s^{-1}}$ are shown in Fig. 7a. The projectile impacts the beam between frames 2 and 3, and in frames 3 and 4 a flexural wave travels from the impact site towards the supports. Subsequently, the beam reaches a maximum deflection and springs back due to the partial reflection of the flexural wave. Core fracture by micro-cracking is evident in frame 4 and an additional core crack initiates at the left-hand support in frame 5. The composite face-sheets remain intact throughout the impact event and the projectile is arrested. The mid-span deflection versus time history measured from the high-speed photographs is plotted in Fig. 7b with the numbers on the curve again corresponding to the frame numbers of Fig. 7a.

The effect of impact velocity upon the deformation mode of the H100 PVC foam core beam can be assessed by comparing Figs. 7a and 8. Fig. 8 displays high-speed photographic sequences (100 μs inter-frame time) of an H2 beam impacted at $v_p = 323\ \mathrm{m\ s^{-1}}$. Impact occurs between frames 1 and 2 and by frame 3 the projectile has fully densified. A number of cracks have initiated in the core by frame 4 and extensive failure of the core due to the coalescence of these cracks is seen in frame 5. The composite faces tear at the supports by frame 5, and this results in complete failure of the beam. The projectile penetrates through the beam without arrest.

Similar deformation mechanisms were observed for the H250 PVC foam core beams but the details are omitted for the sake of brevity.

5.1.3. Balsa wood core sandwich beams

High-speed photographs of an impacted sandwich beam with a balsa wood core (type B2) are shown in Fig. 9. The beam was impacted at $v_p = 140\ \mathrm{m\ s^{-1}}$ by the foam projectile, and the inter-frame time is again 100 μs. The mechanism of deformation is similar to that of the PVC foam core sandwich beams and involves the propagation of a flexural wave along the beam from the impact site towards the supports. In the early stages of motion, vertical cracks form within the balsa core along the *rays* of the balsa wood. Subsequently, these cracks kink into delamination cracks between the core and face-sheets (frame 3) and propagate along the face-sheet/core interface. This delamination of the face-sheets was observed in all the dynamic experiments on balsa wood core sandwich beams. Delamination dramatically reduces the shear stiffness and strength of the sandwich beams, and thereby negates the sandwich effect.

5.2. Comparison of the dynamic strength of the sandwich beams on the basis of equal mass

We proceed to compare the dynamic strengths of beams within each of the Sets 1–3 of Table 1. The maximum mid-span deflection of the back faces of the beams w_{max} is plotted against the projectile momentum I_0 in Fig. 10a–c, for each set in turn. For the sake of clarity we do not include the discrete experimental data points. Rather, best-fitting power law relations between w_{max} and I_0 are fitted to the data of Figs. 4 and 5, and are re-plotted in Fig. 10. Although the power law relations are accurate, we offer no particular physical justification for them. The relative performance of the sandwich beams within each set is summarised as follows.

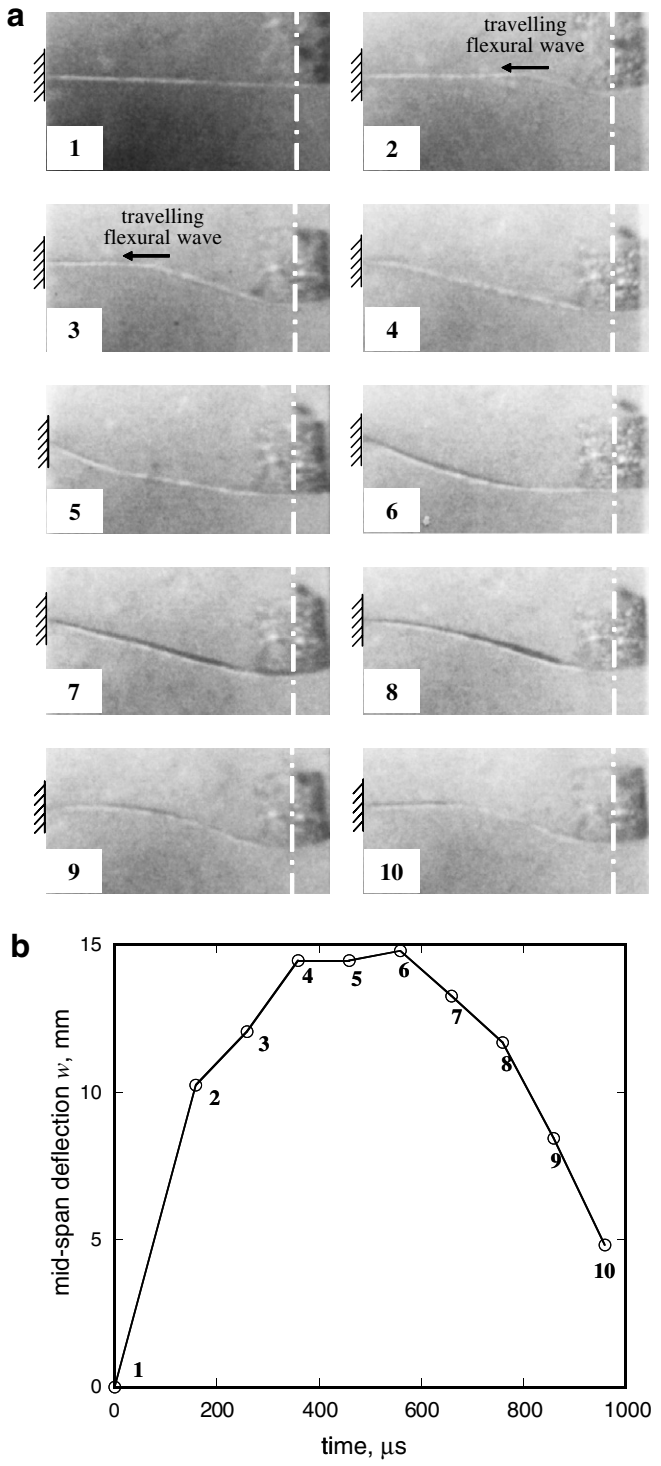

Fig. 6. The deformation of the M1 monolithic beam impacted by the foam projectile at a velocity $v_p = 84\ \mathrm{m\ s^{-1}}$. (a) High-speed photographic sequences at an inter-frame time of 100 μs. (b) The mid-span deflection versus time history extracted from the photographs in (a). The numbers on the curve correspond to the frames in (a).

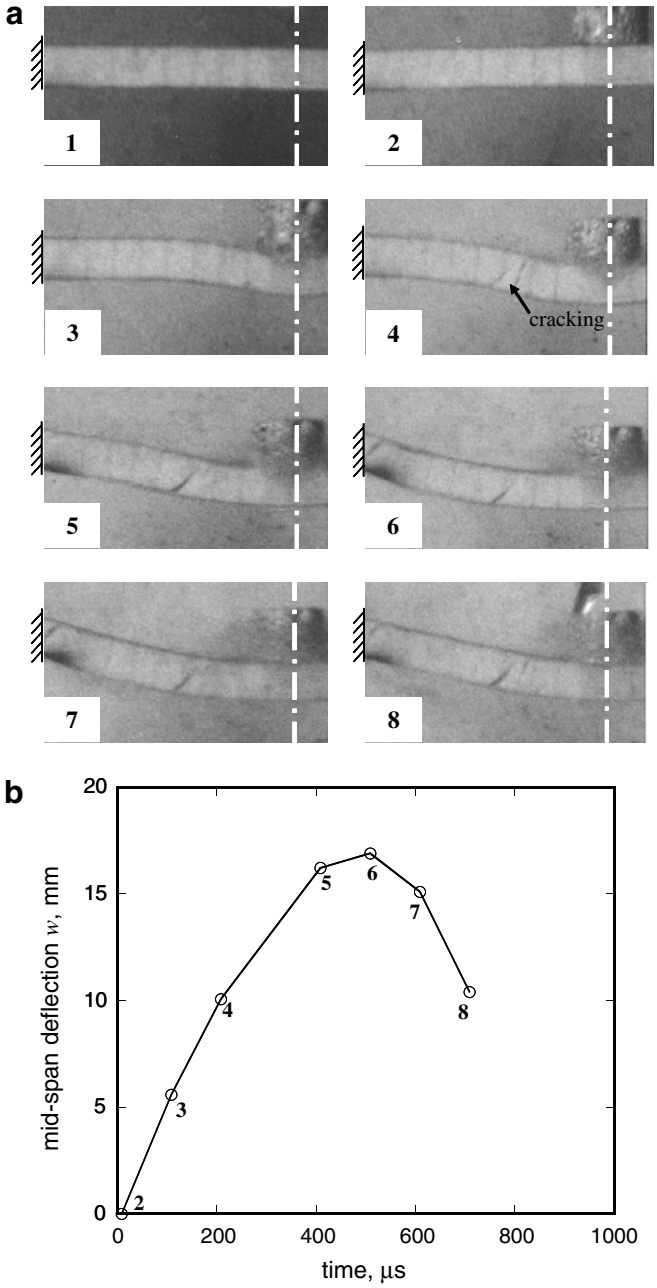

Fig. 7. The deformation of the H2 sandwich beam (H100 PVC foam core) impacted by the foam projectile at a velocity $v_p = 204$ m s^{-1}. (a) High-speed photographic sequences at an inter-frame time of 100 μs. (b) The mid-span deflection versus time history extracted from the photographs in (a). The numbers on the curve correspond to the frames in (a).

5.2.1. Set 1 ($m \approx 3.5$ kg m^{-2}, Fig. 10a)

The H100 foam core beams (H1) outperform the balsa wood core beams (B1) of approximately equal geometry. This confirms that the low shear ductility of the balsa wood core adversely affects its performance. Equal mass monolithic beams have a higher dynamic strength than the balsa wood core sandwich beams but are weaker than the H100 core sandwich beams.

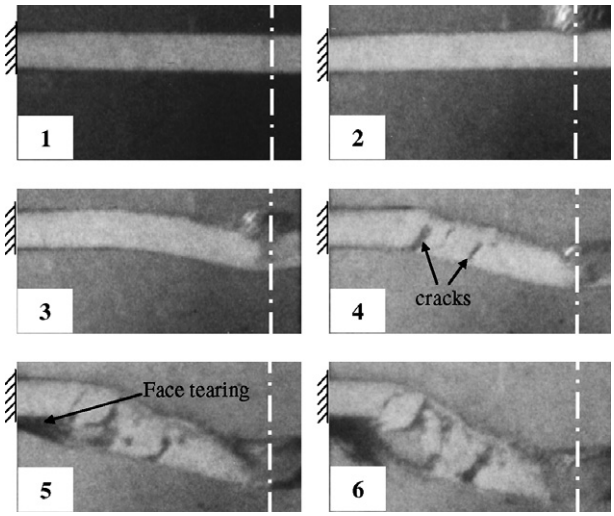

Fig. 8. High-speed photographic sequence of sandwich beam specimen H2 (H100 PVC foam core) impacted by the foam projectile at a velocity $v_p = 323\ \mathrm{m\ s^{-1}}$. The inter-frame time is 100 μs.

5.2.2. Set 2 ($m \approx 4.3\ \mathrm{kg\ m^{-2}}$, Fig. 10b)

The $c = 15$ mm H100 core sandwich beams (H2) have the highest dynamic strength and outperform the $c = 5$ mm H250 foam core beams (HD1). Although the H250 foam has a higher strength, the increased core thickness of the H100 beams gives these beams a higher impact resistance. The $c = 15$ mm balsa wood core beams (B2) outperform the HD1 beams at low values of I_0 but delamination failure of the B2 beams reverses the order at higher impulses.

5.2.3. Set 3 ($m \approx 6.3\ \mathrm{kg\ m^{-2}}$, Fig. 10c)

The HD2 beams have the best performance as they are made from the H250 core of thickness $c = 15$ mm (i.e., the strongest and thickest core). The HD3 and H3 beams have a comparable performance as the higher core thickness of the H3 beams compensates for the lower strength of the H100 foam.

We conclude that sandwich beams can outperform monolithic beams of equal mass. For sandwich beams of equal mass, a trade-off exists between sandwich density and core thickness: a core of high density will be strong and thin, while a low density core will be weak but thick. The increased "sandwich effect" in sandwich beams with low density cores can compensate for the low core strength (e.g., the H2 beams have a higher dynamic strength compared to the HD1 beams). Shear failure of the core can change the order of merit. For example, in Set 2, the B2 beams are weaker than the HD1 beams at high impulse levels, due to shear failure of the brittle balsa wood.

6. Concluding remarks

The dynamic response of composite monolithic and sandwich beams has been measured by loading end-clamped beams at mid-span with metal foam projectiles. The sandwich beams comprise glass-vinylester face-sheets and either a PVC foam (low strength H100 core of density $100\ \mathrm{kg\ m^{-3}}$ or a high strength H250 core of density $250\ \mathrm{kg\ m^{-3}}$) or balsa wood core. High-speed photography was used to measure the transient transverse deflection of the beams and determine the dynamic modes of deformation.

The dynamic deformation mode in both the sandwich and monolithic beams comprises a flexural wave that travels from the impact site to the supports. This wave is partially reflected from the supports, and the maximum deflection of the beam mid-span occurs approximately at the instant that the flexural wave reaches the supports. The failure mechanisms in the PVC sandwich beams include cracking in the core and tensile failure of the face-sheets at the supports. Delamination of the face-sheets from the core is also observed in the balsa wood core beams.

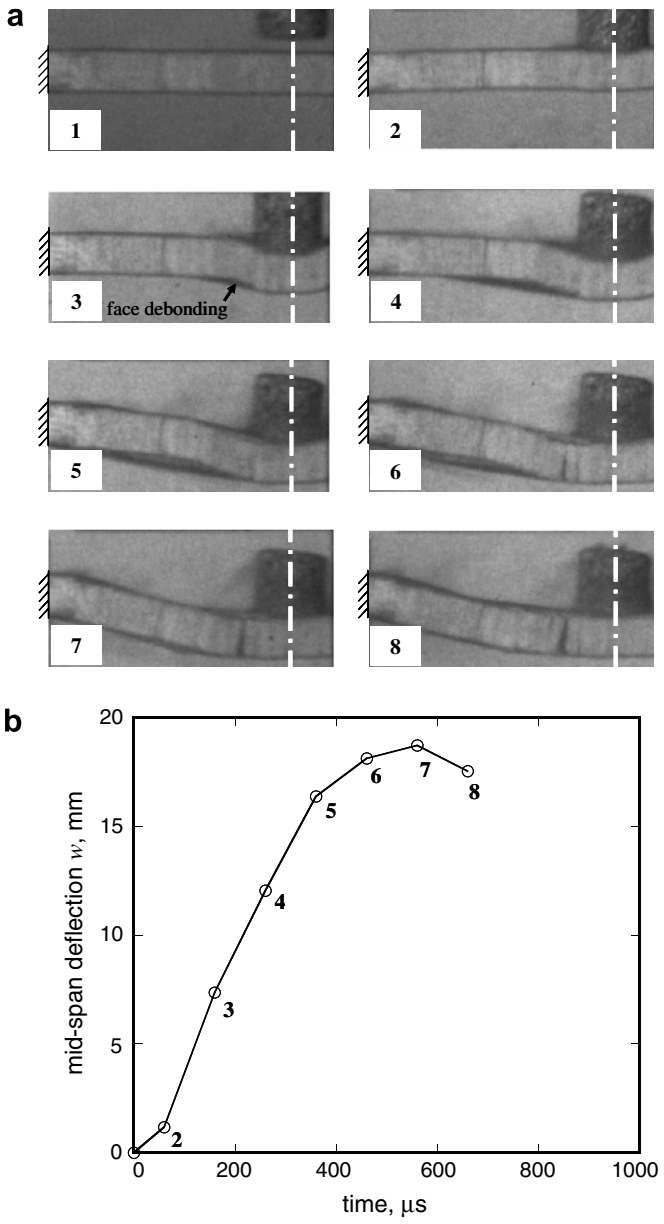

Fig. 9. The deformation of the B2 sandwich beam (balsa wood core) impacted by the foam projectile at a velocity $v_p = 140\ \mathrm{m\ s^{-1}}$. (a) High-speed photographic sequences at an inter-frame time of 100 μs. (b) The mid-span deflection versus time history extracted from the photographs in (a). The numbers on the curve correspond to the frames in (a).

The dynamic resistance of the beams is quantified by the maximum transverse deflection at the mid-span of the beams for a fixed magnitude of projectile momentum. Appropriately designed sandwich beams have a higher dynamic strength than monolithic beams of equal mass. Moreover, we observe that well-designed sandwich beams with the low strength H100 PVC foam core outperform sandwich beams with the high strength H250 PVC foam core. This is attributed to the higher core thicknesses of the H100 core beams. The balsa wood core outperforms the PVC cores at low impulses. However, at sufficiently high impulses, the balsa wood core undergoes shear failure and results in a sandwich beam of low dynamic strength.

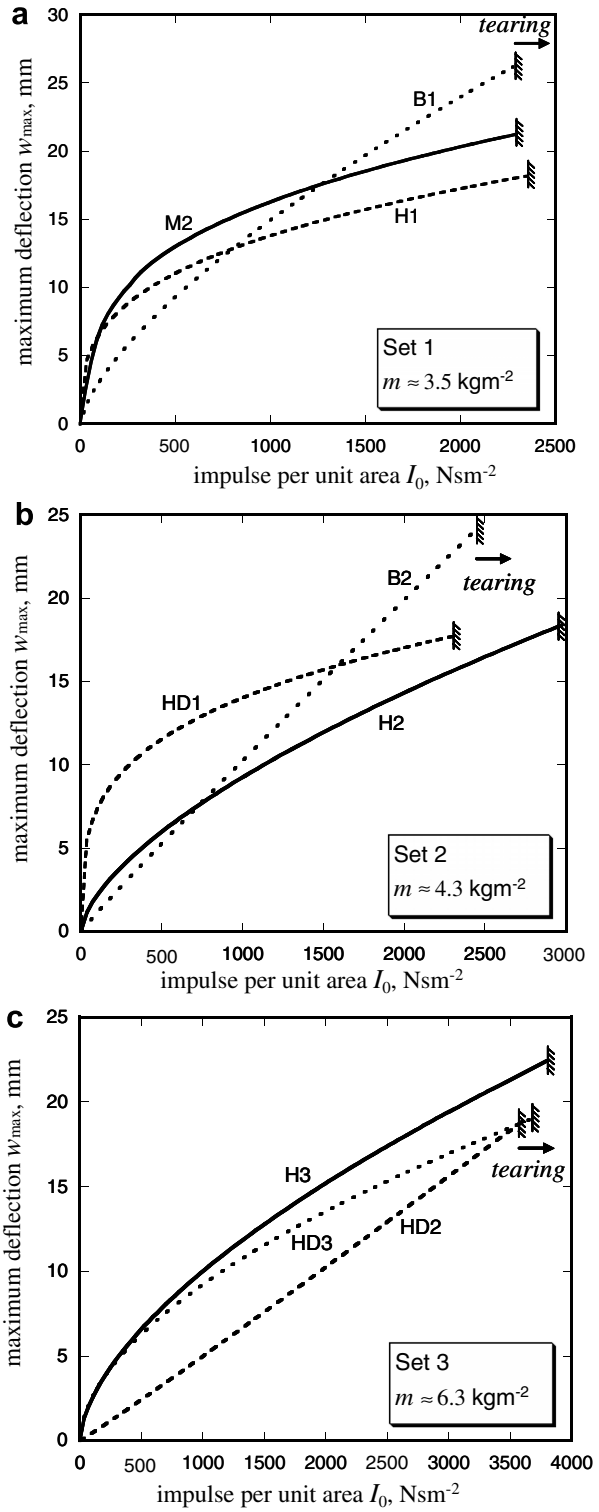

Fig. 10. Comparison of the measured maximum mid-span deflections w_{max} of the back face of sandwich and monolithic beams of equal mass. The deflections w_{max} are plotted as a function of the projectile momentum I_0 for the beams in (a) Set 1, (b) Set 2 and (c) Set 3 of Table 1. For the sake of clarity, only power law fits to the experimental data of Figs. 4 and 5 are included.

Acknowledgements

The authors are grateful to ONR (US Office of Naval Research) for their financial support under contract number 0014-91-J-1916. The authors also are pleased to acknowledge Prof. Dan Zenkert (KTH) and Dr. Darren Radford (CUED) for helpful discussions.

References

Abrate, S., 1997. Localized impact on sandwich structures with laminated facings. Applied Mechanics Reviews 50 (2), 69–82.

Abrate, S., 1998. Impact of Composite Structures. Cambridge University Press, Cambridge.

Ashby, M.F., Evans, A.G., Fleck, N.A., Gibson, L.J., Hutchinson, J.W., Wadley, H.N.G., 2000. Metal Foam: A Design Guide. Butterworth-Heinemann, London.

Deshpande, V.S., Fleck, N.A., 2001. Multi-axial yield behaviour of polymer foams. Acta Materialia 49 (10), 1859–1866.

Fleck, N.A., Deshpande, V.S., 2004. The resistance of clamped sandwich beams to shock loading. Journal of Applied Mechanics, ASME 71, 386–401.

Gibson, L.J., Ashby, M.F., 1997. Cellular Solids: Structure and Properties. Cambridge University Press, Cambridge.

Harding, J., Welsh, L.M., 1983. A tensile testing technique for fibre-reinforced composites at impact rates of strain. Journal of Materials Science 18, 1810–1826.

Mäkinen, K., 2001. Underwater shock loaded sandwich structures. Ph.D. thesis, Royal Institute of Technology, Department of Aeronautics, Stockholm, Sweden.

McShane, G.J., Radford, D.D., Deshpande, V.S., Fleck, N.A., in press. The response of clamped sandwich plates with lattice cores subjected to shock loading. European Journal of Mechanics A: Solids.

Moyer, E.T., Amir, G.G., Olsson, K.A., Hellbratt, S.E., 1991. Response of GRP sandwich structures subjected to shock loading. Sandwich Construction, vol. 2. EMAS.

Olsson, R., Donadon, M.V., Falzon, B.G., 2006. Delamination threshold load for dynamic impact on plates. International Journal of Solids and Structures 43 (10), 3124–3141.

Radford, D.D., Deshpande, V.S., Fleck, N.A., 2005. The use of metal foam projectiles to simulate shock loading on a structure. International Journal of Impact Engineering 31 (9), 1152–1171.

Radford, D.D., Fleck, N.A., Deshpande, V.S., in press. The response of clamped sandwich beams subjected to shock loading. International Journal of Impact Engineering.

Rathbun, H.J., Radford, D.D., Xue, Z., Yang, J., Deshpande, V.S., Fleck, N.A., Hutchinson, J.W., Zok, F.W., Evans, A.G., in press. A dynamic probe for validating simulations of shock loaded metallic sandwich panels. International Journal of Solids and Structures.

Steeves, C.A., Fleck, N.A., 2004. Collapse mechanisms of sandwich beams with composite faces and a foam core, loaded in three-point bending. Part I: analytical models and minimum weight design. International Journal of Mechanical Science 46, 561–583.

Symmonds, P.S., 1954. Large plastic deformation of beams under blast type loading. In: Second US National Congress of Applied Mechanics.

Tagarielli, V.L., Fleck, N.A., Deshpande, V.S., 2004. Collapse of clamped and simply supported composite sandwich beams in three-point bending. Composites B: Engineering 35, 523–534.

Tagarielli, V.L., Deshpande, V.S., Fleck, N.A., Chen, C., 2005. A transversely isotropic model for foams, and its application to the indentation of balsa. International Journal of Mechanical Sciences 47, 666–686.

Tagarielli, V.L., Deshpande, V.S., Fleck, N.A., in press. The uniaxial stress versus strain response of PVC foams and balsa wood at low and high strain rates. Composites B.

Taylor, G.I., 1941. The pressure and impulse of submarine explosion waves on plates. The Scientific Papers of G.I. Taylor, vol. III. Cambridge University Press, 1963, Cambridge, pp. 287–303.

Wang, A.J., Hopkins, H.G., 1954. On the plastic deformation of built-in circular plates under impulsive load. Journal of Mechanics and Physics of Solids 3, 22–37.

Xu, L.R., Rosakis, A.J., 2000. Real time experimental investigation of dynamic failure mode selection in sandwich structures. In: Proceedings of the ASME Mechanical Engineering Congress and Exposition, Orlando, FL – Mechanics of Sandwich Structures, AMD, vol. 245.

Xue, Z., Hutchinson, J.W., 2003. Preliminary assessment of sandwich plates subject to blast loads. International Journal of Mechanical Sciences 45, 687–705.

Zenkert, D., 1995. An Introduction to Sandwich Construction. EMAS.